OPEN ACCESS   Check for updates

Intermetallic-strengthened nanocrystalline bainitic steel

C. N. Hulme-Smith ⓘ*, S. W. Ooi ⓘ and H. K. D. H. Bhadeshia

Department of Materials Science and Metallurgy, University of Cambridge, Cambridge, UK

ABSTRACT
A new thermally stable, nanocrystalline bainitic steel has been developed, rich in nickel and aluminium. During tempering, it is expected that a significant quantity of intermetallic precipitates will form. This was confirmed by X-ray diffractometry, scanning transmission electron microscopy, Fourier transform analysis of atomic column images, energy dispersive X-ray spectroscopy and selected area electron diffraction. These are the first intermetallics to be produced in a nanocrystalline bainitic steel.

A novel nanocrystalline bainitic steel has been developed to resist the thermal decomposition of austenite during exposure to high temperatures [1]. The alloy (composition in Table 1) was able to survive heating to 600°C for 1 h without a catastrophic change in microstructure. Steels with comparable levels of nickel and aluminium can form β-(Ni, Fe) Al precipitates during tempering at 700–900°C [2–4].

Thermodynamic modelling was performed using the software MTData (National Physical Laboratory, Teddington, U.K.) [5], with the SGTE database version 4.2 to predict the stable phases as a function of temperature (Figure 1). An ordered cubic phase (primitive with a motif of (Fe, Ni) at (0,0,0) and Al at ((1/2),(1/2),(1/2))) is expected to form at ≤ 800°C. The calculated composition of this phase is approximately $(Fe_{0.5}Ni_{0.5})Al$.

A block measuring approximately $40\,mm \times 80\,mm \times 20\,mm$ was austenitised at 1000°C for 1 h and held at 250 ± 1°C for 120 h to form the maximum possible fraction of bainitic ferrite. This formed a homogeneous structure of nanostructured bainitic ferrite platelets, retained austenite films and retained austenite blocks [1].

As-transformed material was cut using electro discharge machining to 2 mm diameter and 40 mm length. The surface oxide was ground off and the sample cut to a length of 25 mm, for analysis using synchrotron X-ray diffraction at beamline I12 at Diamond Light Source, Didcot, U.K. The sample was continuously illuminated with a 0.5 mm × 0.5 mm beam of 120 keV X-rays, detected using a Thales Pixium RF4343 2D detector with 148 μm × 148 μm pixels positioned perpendicular to the X-ray beam and approximately 1500 mm from the sample. The sample was heated in a halogen lamp furnace at $10°\,min^{-1}$ to 500°C whereupon the temperature was kept constant until the diffraction rings were observed to stop changing. The sample was then allowed to cool at a maximum rate of $20°\,min^{-1}$ to ambient temperature. Detector calibration was by a ceria standard.

Subsequently, a second sample of as-transformed material was cut and tempered at 500 ± 1°C for 1 h to replicate the synchrotron experiment. 3 mm diameter foils were produced and ground to a thickness of ≤ 50 μm and electropolished to perforation using a Struers TenuPol-5 twin-jet electropolishing machine in 5% perchloric acid, 25% glycerol and 70% ethanol at 25 V and approximately 10°C. Imaging and selected area diffraction were performed on an FEI Tecnai Osiris 80-200 transmission electron microscope. The selected area diffraction patterns of one region (supplemental Figure 1) show spots consistent with austenite viewed down a $\langle 100 \rangle$ zone axis (supplemental Figure 2), ferrite and/or β-(Ni, Fe) Al viewed down a $\langle 20\bar{1} \rangle$ zone axis (supplmental Figure 3) and cementite viewed down $[1.40\,1.05\,0.\bar{3}5]$ (supplemental Figure 4). Atomic column images were taken using an FEI Titan³ 80–300 transmission electron microscope (Figure 2). Fourier transform analysis using the software ImageJ [6] of a region of ferrite that incorporated precipitates approximately 5 nm in diameter revealed that the matrix exhibited plane spacings of (2.06 ± 0.08)Å, consistent with both α_{110} and β_{110} [3,4]. While most precipitates showed spacings similar to the matrix, a small

---

CONTACT C. N. Hulme-Smith ✉ chrihs@kth.se ⊘ https://www.linkedin.com/in/christopher-hulme-smith-bb770514a ⊡ Department of Materials Science and Metallurgy, University of Cambridge, 27 Charles Babbage Road, Cambridge CB3 0FS, UK
*Present address: KTH Royal Institute of Technology, School of Industrial Engineering and Management, Department of Materials Science and Engineering, Brinellvägen 23, SE-100 44 Stockholm, Sweden.

Table 1. Measured composition of the alloy studied.

C	Mn	Al	Ni	Co	Mo
0.45	0.15	2.63	13.2	3.99	0.30

Note: All values are wt-% and the residue is iron.

number exhibited larger spacings: (2.74 ± 0.09)Å, very close to the lattice parameter of β-(Ni, Fe) Al. Only precipitates where the zone axis is $\langle 100 \rangle$ will exhibit the large plane spacing. This explains the fact that not many precipitates exhibit the large plane spacing.

Following the synchrotron heat treatment, the final diffractogram was integrated. Austenite and ferrite peaks are present, along with other smaller peaks (Figure 3). Most of these could be attributed to cementite, but the peak at 2.1°, equivalent to a plane spacing of 2.886 Å, could not. This is very close to the ferrite 100 plane spacing (2.888 Å). Teng et al. showed that the precipitation of β-(Ni, Fe) Al in ferrite leads to a peak at this precise position [4]. β-(Ni, Fe) Al may not be definitively identified using XRD as the majority of peaks overlap those due to ferrite (Figure 3). Only the 100 peak is visible and so relative peak intensities, and therefore the structure factor, may not be investigated.

Energy dispersive X-ray spectroscopy in a ferrite plate reveals that the fine precipitates are enriched relative to the matrix in both nickel and aluminium and deficient in iron and cobalt (Figure 4). Since the sample thickness is unknown, it is not possible to determine the composition of the precipitate using EDX; however, both nickel and aluminium are enriched in areas containing precipitates, suggesting that the precipitates are significantly enriched in both elements.

The structure consists of austenite and ferrite with fine precipitates embedded in the latter and coarser cementite particles throughout (supplemental Figure 1). Electron diffraction reveals strong spots attributable to ferrite, a series of weak spots that are attributed to an apparent ferrite 100 reflexion (supplemental Figure 2), a series of spots fitted by austenite (supplemental Figure 3) and spots fitted by cementite (supplemental Figure 4).

Prior to tempering, the alloy is known to consist of retained austenite and bainitic ferrite [1] only with no intermetallic phases. This is expected, since the low mobility of substitutional solutes at the bainite transformation temperature slows diffusion to such an extent that this type of preciptiate does not form. The X-ray diffractogram (Figure 3) contains peaks associated with both of these phases, as well as cementite and β-(Ni, Fe) Al. The precipitation of cementite is expected due to the high degree of carbon supersaturation following the bainite transformation [1,7]. The formation of β-(Ni, Fe) Al is both expected from thermodynamic calculations (Figure 1) and consistent with other steels with high nickel and aluminium contents [2–4].

The presence of the B2-ordered β phase should provide strengthening at all temperatures, imparting
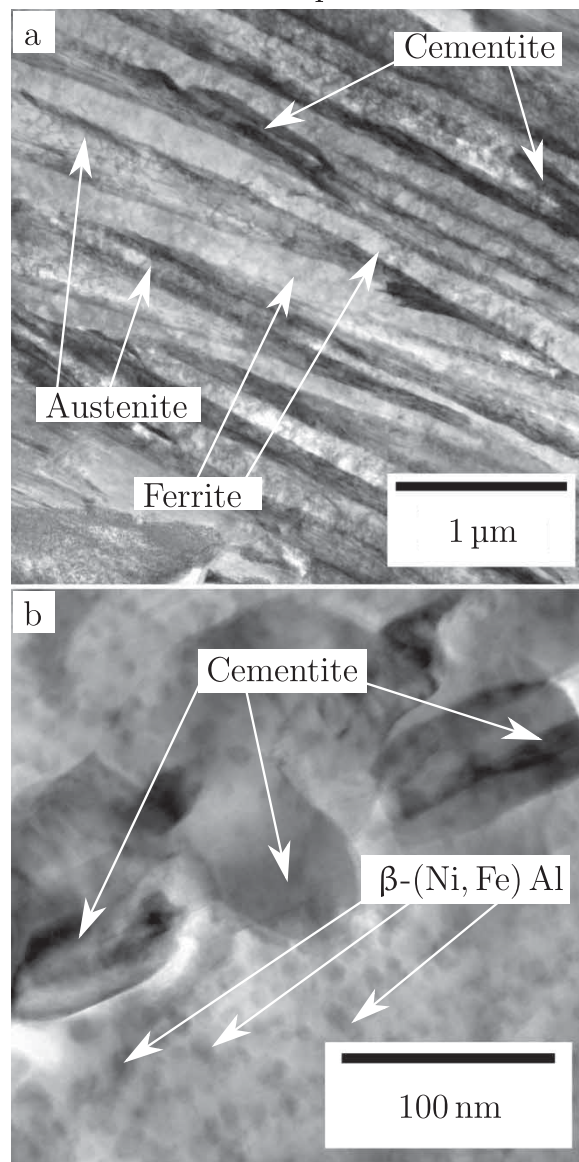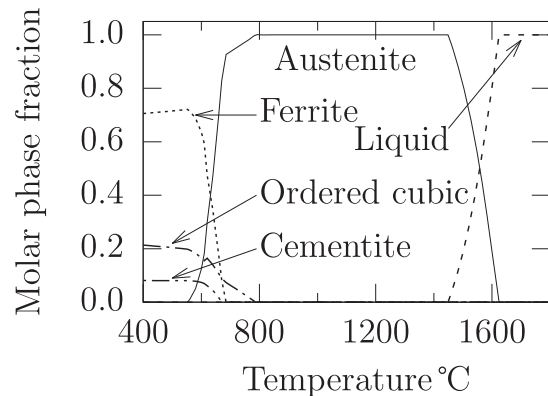

Figure 1. Phases that are calculated to be thermodynamically stable when liquid, austenite, ferrite, and cementite and a B2-ordered cubic phase only are allowed. Micrographs before and after tempering show that the film structure found in the as-transformed material survives tempering. Full-size micrographs are available as supplementary Figures 5 and 6.

creep resistance, and the lattice parameter is well-matched to the matrix phase [2,4]. The current alloy exhibits a hardness of 446 ± 3HV30 after the bainite transformation and 557 ± 3HV30 after the tempering
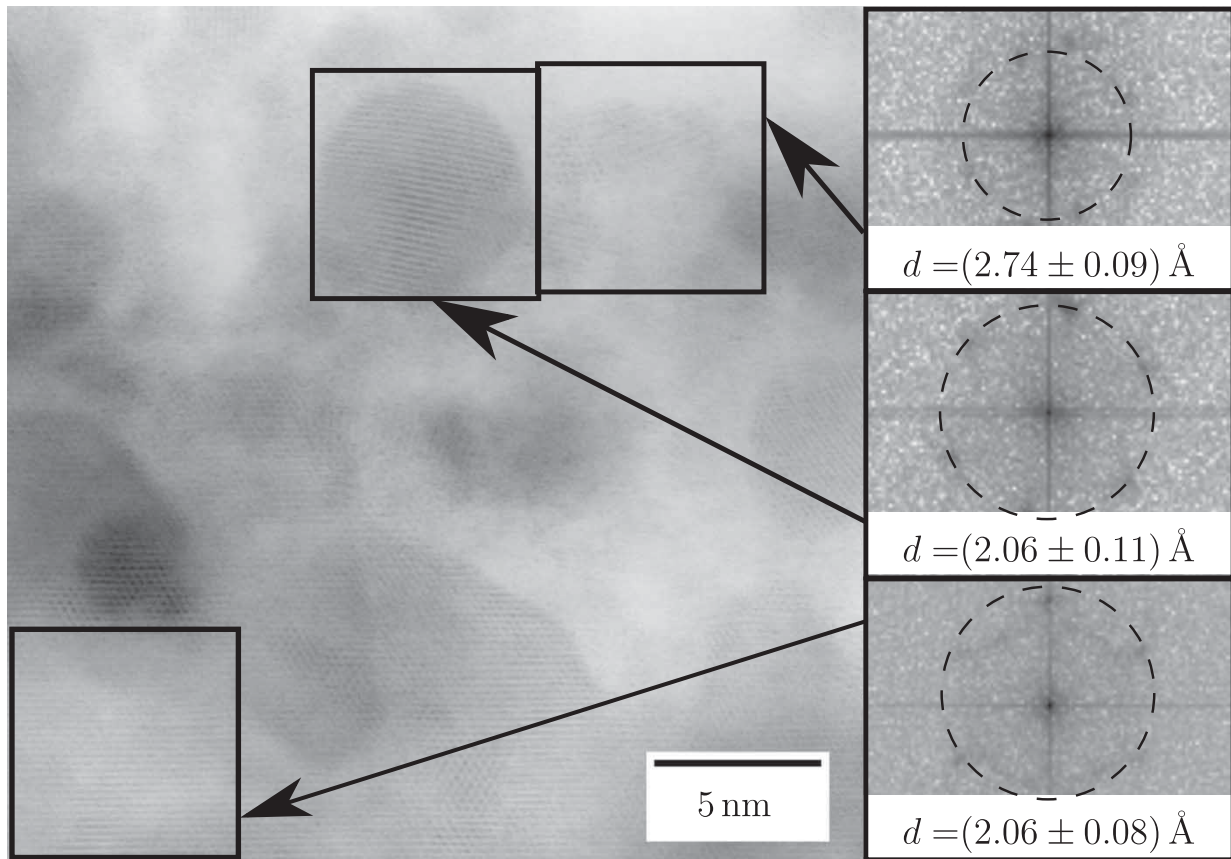
Figure 2. Transmission electron micrograph of material after tempering at 480°C for 8 d showing atomic columns. Fourier transforms of the marked regions are given, together with the apparent lattice spacings of the points that lie on the marked circles. The top Fourier transform shows a plane spacing consistent with d_{100} of ferrite and $\beta-(\text{Ni, Fe})$ Al. The other two Fourier transforms exhibit plane spacings consistent with d_{110} of both phases. Uncertainties were calculated assuming that the most significant source of error was determining the location of the centre of each spot in the Fourier transform. The uncertainty is derived by assuming that the centre may only be determined to within one pixel.
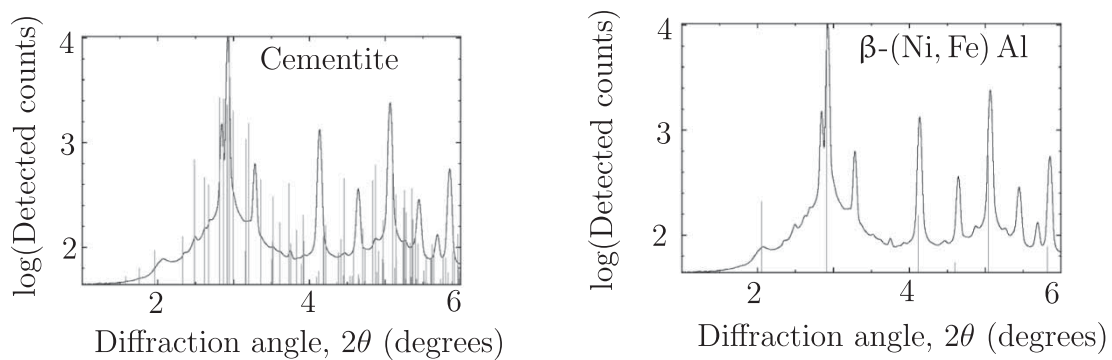

Figure 3. Synchrotron X-ray diffractogram of sample transformed at 250°C and tempered at 500°C for 1 h. Most small peaks correspond to those of cementite. However, this is not true of the peak at 2.1, which is consistent with β-(Ni, Fe) Al. The large peaks are fitted by austenite and ferrite.

treatment described above. This is in contrast to previous bulk nanocrystalline bainitic steels in literature, which undergo cementite precipitation and the transformation of austenite to ferrite during tempering, but do not precipitate intermetallic particles [8]. These previously reported alloys are softened significantly by tempering. Further research in this area is recommended.

In conclusion, a nanostructured bainitic steel with high concentrations of both nickel and aluminium has been tempered under conditions similar to those in gas and steam turbines and it has been shown that particles of intermetallic precipitates are formed. Despite the prolonged heat treatment necessary for the production of this intermetallic phase, austenite has survived and should provide exceptional toughness. Such
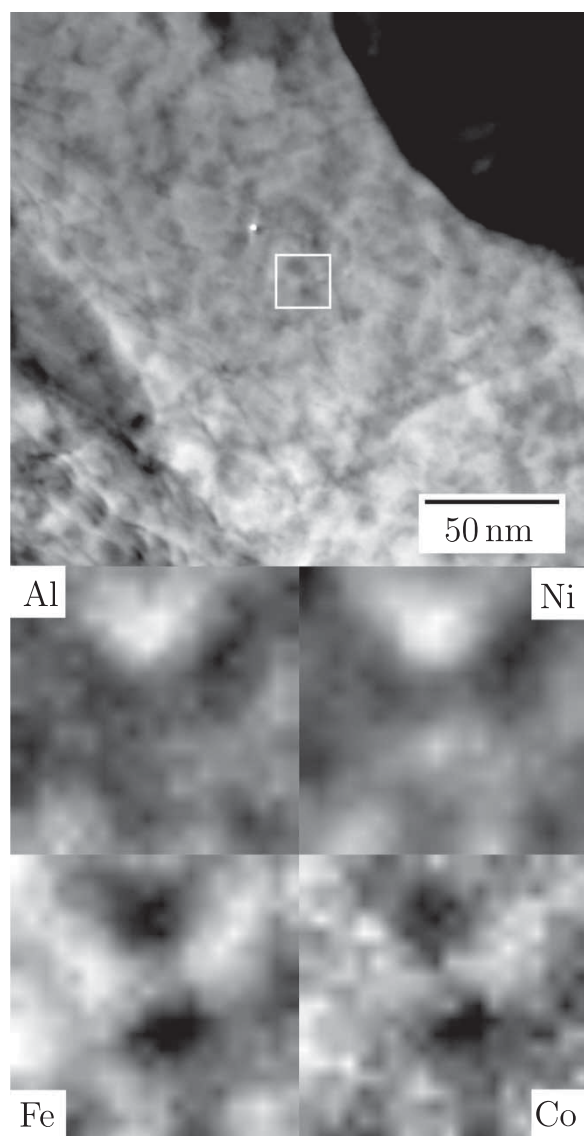
Figure 4. Bright field micrograph of ferrite and EDX element maps from the marked region. Elemental maps are from a content of zero (black) to the maximum for each element (white). Enriched regions of aluminium and nickel coincide.

a combination of two major phases and intermetallic precipitates has never before been obtained in bainitic steel.

Disclosure statement

No potential conflict of interest was reported by the authors.

ORCID

C. N. Hulme-Smith http://orcid.org/0000-0002-6339-4612
S. W. Ooi http://orcid.org/0000-0001-8415-0214

References

[1] Hulme-Smith CN, Ooi SW, Bhadeshia HKDH. Mechanical properties of thermally-stable, nanocrystalline bainitic steels. Mater Sci Eng A. 2017;700:714–720.

[2] Stallybrass C, Schneider A, Sauthoff G. The strengthening effect of (Ni,Fe)Al precipitates on the mechanical properties at high temperatures of ferritic Fe–Al–Ni–Cr alloys. Intermetallics. 2005;13:1263–1268.

[3] Teng ZK, Miller MK, Ghosh G, et al. Characterization of nanoscale NiAl-type precipitates in a ferritic steel by electron microscopy and atom probe tomography. Scr Mater. 2010;63:61–64.

[4] Teng ZK, Ghosh G, Miller MK, et al. Neutron-diffraction study and modeling of the lattice parameters of a NiAl-precipitate-strengthened Fe-based alloy. Acta Mater. 2012;60:5362–5369.

[5] Davies RH, Dinsdale AT, Gisby JA. MTDATA - Thermodynamic and phase equilibrium software from the national physical laboratory. CALPHAD. 2002;26:229–271.

[6] Schneider CA, Rasband WS, Elicieri KW. NIH Image to ImageJ: 25 years of image analysis. Nat Methods. 2012;9:671–675.

[7] Saha Podder A, Bhadeshia HKDH. Thermal stability of austenite retained in bainitic steels. Mater Sci Eng A. 2010;527:2121–2128.

[8] García-Mateo C, Peet MJ, Caballero FG, et al. Tempering of hard mixture of bainitic ferrite and austenite. Mater Sci Technol. 2004;20:814–818.